Supplementary Information for

Space-Time Decoupled Information Metasurface Integrating Reflective Mixer and Phase Shifter Functions

Xuehui Dong[1], Miyu Feng[1], Bokai Lai[1], Chen Shao[1],Jianan Zhang[1], Rujing Xiong[1], Kai Wan[1], Tiebin Mi[1, *], Robert Caiming Qiu[1, *]

1 School of Electronic Information and Communication Engineering, Huazhong University of Science and Technology, Wuhan 430000, China

* Correspondence should be addressed to Tiebin Mi and Robert Caiming Qiu.

Emails: mitiebin@hust.edu.cn; caiming@hust.edu.cn

This supplementary information contains the following sections:

Supplementary Note 1. Theoretical analysis of space-time decoupled metasurface

Supplementary Note 2. Distortion Analysis

Supplementary Note 3. Circuits analysis of distortion and high-rate modulation

Supplementary Note 4. Analysis of 1-bit quantification of phase factor in terms of beamforming

Supplementary Note 5. Received waveforms and our designed UI of system

Descriptions about Video Demos:

Video 1. Single input: arbitrary waveform modulation by STD-Metasurface

Video 2. Over-the-air combination of two scaled waveforms

Video 3. Simultaneous beamforming and modulation

Video 4. Backscatter communication and Micro-Doppler signature generation

Supplementary Note 1. Theoretical analysis of space-time decoupled metasurface

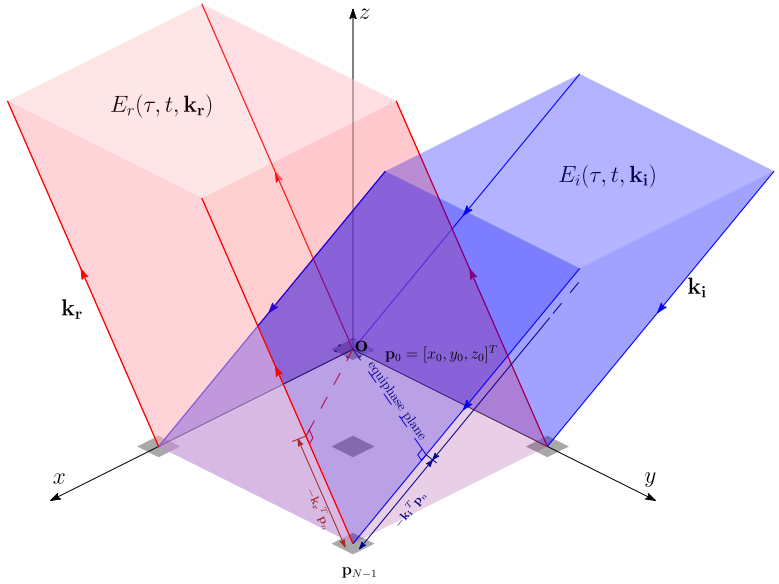

Supplementary Figure 1

Firstly, we express the general reflection coefficients (GRC) as the variable in fast-time domain τ and slow-time-domain t,

$$\Gamma_n(\tau, t) = \gamma_n(\tau)e^{j\theta_n(t)}. \tag{1}$$

The fast-domain component $\gamma_n(\tau) \in \mathbb{C}$ represents the modulation factors, in general, denoting any electromagnetic (EM) characteristics in EM wave that can be swiftly manipulated by reconfigurable metamaterials, such as phase, amplitude, polarizations, or complex envelope so on. The slow-domain component $e^{j\theta_n(t)}$ presents the skewing between the incident wave and reflected wave, and the surface distribution of phase factors denoted by $\mathbf{w(t)} = \left[e^{j\theta_0(t)}, e^{j\theta_1(t)}, \ldots, e^{j\theta_{N-1}(t)}\right]^T$. Here we define two critical vectors, EM characteristics vector $\boldsymbol{\varepsilon}(\tau, t)$ and manifold vector of reflected array $\mathbf{v}(\mathbf{k_r}, \mathbf{k_i}; \mathbf{P})$. The former determinates all the programmable EM characteristics, the latter determinates the size and shape of reflected array,

$$\boldsymbol{\varepsilon}(\tau, t) = \begin{bmatrix} \Gamma_0(\tau, t) \\ \Gamma_1(\tau, t) \\ \vdots \\ \Gamma_{N-1}(\tau, t) \end{bmatrix}, \mathbf{v}(\mathbf{k_r}, \mathbf{k_i}; \mathbf{P}) = \begin{bmatrix} e^{-j(\mathbf{k_r}-\mathbf{k_i})^T\mathbf{p_0}} \\ e^{-j(\mathbf{k_r}-\mathbf{k_i})^T\mathbf{p_1}} \\ \vdots \\ e^{-j(\mathbf{k_r}-\mathbf{k_i})^T\mathbf{p_{N-1}}} \end{bmatrix}, \tag{2}$$

where $\mathbf{k_r}$ and $\mathbf{k_i}$ respectively denotes the wavenumber vector of reflected wave and incident wave. The wavenumber vector can be expressed as $\mathbf{k} = -\frac{2\pi}{\lambda}[\sin\theta\cos\phi\ \sin\theta\sin\phi\ \cos\theta]^T$. Here we have assumed, without loss of generality,

that both incoming and reflected/outgoing waves are plane waves. If the case of near-field spherical waves is considered, it is only necessary that the unit-oriented vector difference $(\mathbf{k_r} - \mathbf{k_i})$ in $\mathbf{v}(\mathbf{k_r}, \mathbf{k_i}; \mathbf{P})$ be changed to a joint expression in the angular-distance domain. Each column in the matrix $\mathbf{P}$ represents the centre coordinates of each array element. Given a specific $\mathbf{P}$, we can obtain the space-time transfer function (STTF) of metasurface

$$\mathcal{T}_{STD}(\tau, t, \mathbf{k_r}, \mathbf{k_i}) = \boldsymbol{\varepsilon}^T(\tau, t)\mathbf{v}(\mathbf{k_r}, \mathbf{k_i}). \tag{3}$$

Eq.(3) expresses the mapping from the energy distribution of the incident wave to the energy distribution of the outgoing wave in the beam domain at the moment (τ, t), also the time-domain variability of the relationship between an incident wave and an outgoing wave for a given direction pair of the wave. So that the relationship between the incident electric fields and reflected electric fields

$$E_r(\tau, t, \mathbf{k_r}) = \iint \mathrm{d}\mathbf{k_i} \cdot \mathcal{T}_{STD}(\tau, t, \mathbf{k_r}, \mathbf{k_i}) E_i(\tau, t, \mathbf{k_i}) \tag{4}$$

where $E_{i/r}(\tau, t, \mathbf{k_{i/r}}) = E_{i/r}\left(\tau, t, k_{i/r}^x, k_{i/r}^y\right)$ is the Fourier transform of $\hat{E}_{i/r}(\tau, t, x, y)$, and the hat denotes the functions in the Euclidean space, as

$$E_{i/r}\left(\tau, t, k_{i/r}^x, k_{i/r}^y\right) = \left(\frac{1}{2\pi}\right)^2 \iint dxdy\hat{E}_{i/r}(\tau, t, x, y)e^{-j\left(k_{i/r}^x x + k_{i/r}^y y\right)}$$

During one unit time in the slow time domain, the surface distribution of phase factors $\mathbf{w} = \left[e^{j\theta_0}, e^{j\theta_1}, \ldots, e^{j\theta_{N-1}}\right]^T$ remains unchanged. Assuming that the bandwidth B_m of modulation factors is much smaller than $\frac{c}{\lambda}$, the Eq. (4) can be expressed as

$$E_r(\tau, \mathbf{k_r}) = \tilde{E}_r(\tau)\bar{E}_r(\mathbf{k_r}) = \underbrace{\tilde{E}_i(\tau)\sum_{n=1}^{N}\gamma_n(\tau)}_{\text{signal modulator}} \cdot \underbrace{\iint \mathrm{d}\mathbf{k_i} \cdot \mathbf{w}^T\mathbf{v}(\mathbf{k_r}, \mathbf{k_i})\bar{E}_i(\mathbf{k_i})}_{\text{beamforming controller}} \tag{5}$$

where the $\tilde{E}(\tau)$ and $\bar{E}(\mathbf{k})$ respectively denotes the time-varying and space-varying parts of electric fields.

Here we give the definitions of space-time coupling metasurface (STC-Metasurface) and space-time decoupling metasurface (STD-Metasurface). A sufficient condition of space-time decoupling (STD) for metasurfaces is also proposed.

Definition 1 (STD-Metasurface): *Given the incident electric fields* $E_i(\tau, \mathbf{k_i})$ *and the manifold vector of metasurface* $\mathbf{v}(\mathbf{k_r}, \mathbf{k_i}; \mathbf{P})$ *defined in (2), the metasurface is called STD-Metasurface if and only if*

$$\mathbb{P}_{\boldsymbol{\varepsilon}}\left[\tilde{E}_r(\tau), \bar{E}_r(\mathbf{k_r})\right] = \mathbb{P}_{\boldsymbol{\varepsilon}}\left[\tilde{E}_r(\tau)\right] \cdot \mathbb{P}_{\boldsymbol{\varepsilon}}[\bar{E}_r(\mathbf{k_r})] \tag{6}$$

where $\mathbb{P}_{\boldsymbol{\varepsilon}}[\cdot]$ *is the probability distribution function (PDF) related to EM characteristics vector defined in (2), and* $\mathbb{P}_{\boldsymbol{\varepsilon}}[\cdot,\cdot]$ *is the jointly PDF.*

Definition 2 (STC-Metasurface): *Given the incident electric fields* $E_i(\tau, \mathbf{k_i})$ *and the manifold vector of metasurface* $\mathbf{v}(\mathbf{k_r}, \mathbf{k_i}; \mathbf{P})$ *defined in (2), the metasurface is called* ***STC-Metasurface*** *if and only if*

$$\mathbb{P}_{\boldsymbol{\varepsilon}}\left[\tilde{E}_r(\tau), \bar{E}_r(\mathbf{k_r})\right] \neq \mathbb{P}_{\boldsymbol{\varepsilon}}\left[\tilde{E}_r(\tau)\right] \cdot \mathbb{P}_{\boldsymbol{\varepsilon}}[\bar{E}_r(\mathbf{k_r})] \tag{7}$$

where $\mathbb{P}_{\boldsymbol{\varepsilon}}[\cdot]$ *is the probability distribution function (PDF) related to EM characteristics vector defined in (2), and* $\mathbb{P}_{\boldsymbol{\varepsilon}}[\cdot,\cdot]$ *is the jointly PDF.*

Theorem 1 (sufficient condition of STD): *If the modulation factors and phase factors of each unit of metasurface are independent, i.e.,*

$$\mathbb{P}\left[\gamma_n, e^{j\theta_n}\right] = \mathbb{P}[\gamma_n] \cdot \mathbb{P}\left[e^{j\theta_n}\right] \tag{8}$$

for n=1…, N, then the Eq. (6) holds.

Proof: According to Eq. (5), we know that $\tilde{E}_r$ and $\bar{E}_r$ are respectively the measurable functions of $\{\gamma_n\}_N$ and $\{e^{j\theta_n}\}_N$, denoted as $\tilde{E}_r = f_1(\boldsymbol{\gamma})$ and $\bar{E}_r = f_2(\boldsymbol{w})$. $\forall u, v \in \mathbb{R}$, the sets $\{\boldsymbol{\gamma} \in \mathbb{C}^{\boldsymbol{N}}: \|f_1(\boldsymbol{\gamma})\| < u\}$ and $\{\boldsymbol{w} \in \mathbb{C}^{\boldsymbol{N}}: \|f_2(\boldsymbol{w})\| < v\}$ are measurable. Also $f_1(\cdot)$ and $f_2(\cdot)$ do not share any common variable. So that the independence of $\boldsymbol{w}$ and $\boldsymbol{\gamma}$ is sufficient for the independence of $\tilde{E}_r$ and $\bar{E}_r$.

■

Remark 1: According to theorem 1, we need to increase the degree-of-freedom (DoF) of control of unit in metasurface to achieve the independent manipulation of both modulation factors and phase factors.

Supplementary Note 2. Distortion Analysis

In traditional transmitters, signal distortion due to nonlinearity primarily originates from the operation of the power amplifier (PA) near its saturation region, where nonlinear effects are significant. In contrast, in STD-Metasurfaces, the nonlinearity of the baseband signal mainly arises from the higher-order derivatives (second-order or higher) of the dynamic DC characteristic of the diode.

Supplementary Figure 2 The distorted waveforms received by the direct-RF-sampling oscilloscope when the baseband inputs of STD-Metasurface are asymmetric sawtooth waveforms with different high levels. (720mV, 820mV, 1120mV).

In the unit circuit of our design, as shown in Fig. 2(c) of the main text, the diode's terminal voltage operates within the range of 0.76 V to 0.82 V. The measured dynamic range of the input voltage at the port is 500 mV to 610 mV, ensuring approximately 65%

modulation efficiency. This means that 65% of the energy of the reflected EM waves carries additional modulated information, while the remaining 35% of the energy retains the information carried by the incident wave. When the amplitude of the port input signal exceeds a certain threshold, the baseband signal begins to deform, resulting in non-linear distortion (see Supplementary Figure 2).

Supplementary Note 3. Circuits analysis of distortion and high-rate modulation

(1) The forward current characteristics of PIN diode

In this work, we use a PIN diode as the non-linear component, where the charge and discharge rates cannot keep up with the rapidly changing bias voltage due to the principle of the PIN diode. A PIN diode comprises an intrinsic (lightly doped) layer situated between the p-type and n-type semiconductor layers. In the context of small-signal modulation, the conduction mechanism of the PIN diode is contingent upon the accumulation of minority carriers under forward bias. This process inherently limits the fast response of the small signal, introducing a noticeable delay.

In order to meet the requirements of high-frequency modulation applications, it is necessary to replace the PIN diode with a Schottky diode, which exhibits superior high-frequency performance. The Schottky diode relies on a metal-semiconductor junction and conducts through majority carriers only. It features a lower forward voltage, excellent linearity, and is highly suitable for high-speed modulation applications.

(2) The frequency response of the equivalent RLC circuits

The control circuit operates essentially as an RLC circuit (as shown in Fig. 2(b) in the main text). The circuit inherently exhibits time dispersion effects which manifest themselves in the frequency domain as a specific frequency selectivity. In order to increase the bandwidth, it is essential to ensure that the RLC circuit maintains a flat response within the operating frequency range under the dynamic variation conditions of the diode. This involves optimizing the circuit parameters to minimize impedance variations and achieve uniform performance across the desired frequency spectrum.

Supplementary Note 4. Analysis of 1-bit quantification of phase factor in terms of beamforming

For periodic reflective arrays such as metasurfaces, 1-bit phase quantization will produce the grating lobe assuming planar waves. For applications such as transmitters, the grating lobe is not expected. Here we show that the grating lobe disappears when the air-fed source is close enough to the metasurface (see the rows in Supplementary Figure 3). We present four different settings where the distance between the air-fed source and the metasurface is 0.5, 1, 2, 4 meters from the top row to the bottom row. The first column in Supplementary Figure 3 shows the optimal 1-bit phase distributions, also codebooks, obtained by our proposed algorithm [1].

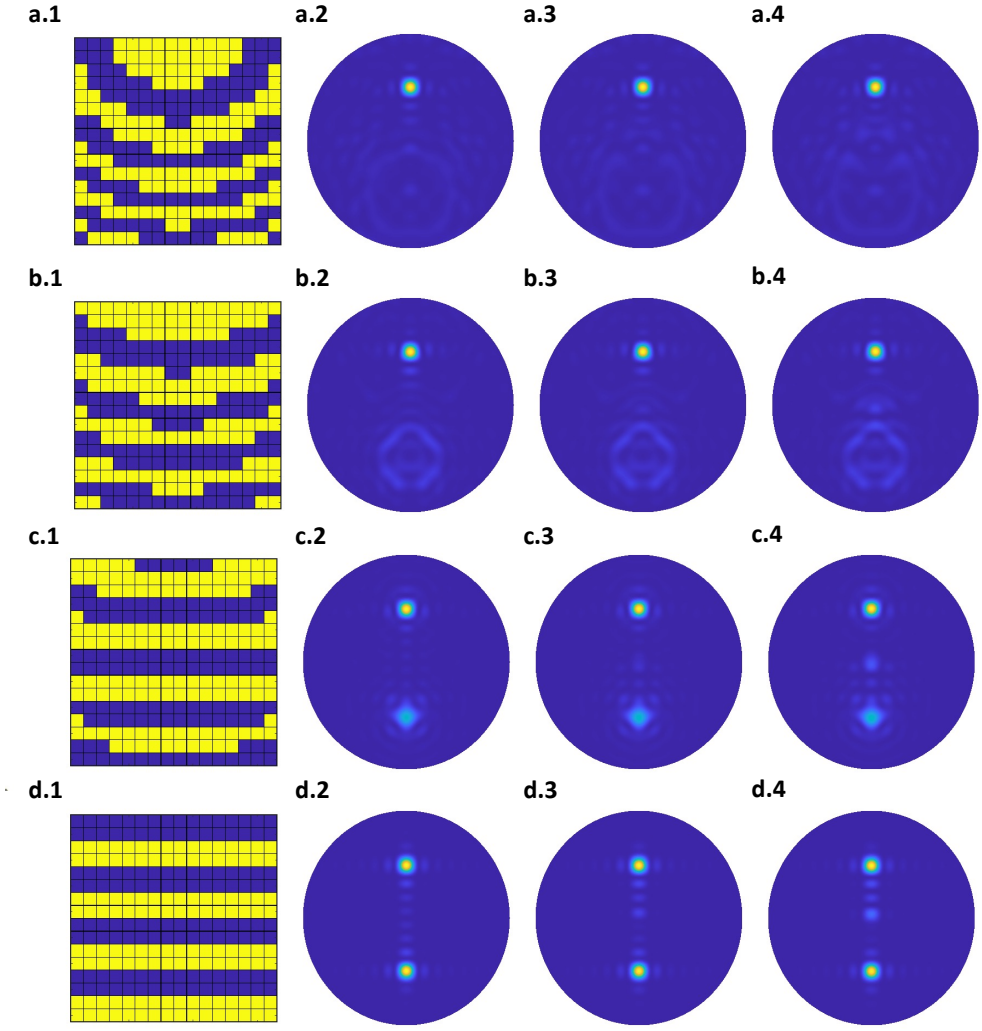

Supplementary Figure 3 The optimal codebooks and corresponding radiation patterns under different distance air-fed source (rows) and different phase biases (columns).

In addition, we also show that the beam patterns show minimal variations when the

phase jitter remains below 30° in the "ON-state" (see the rows in Supplementary Figure 3 and Supplementary Figure 4). The ON state means that the PIN diode is conducting. The second column represents the relative phases of the "ON" and "OFF" states, which are 180° and 0°. The third and fourth columns represent the relative phases of the "ON-state" of 165° and 150° respectively.

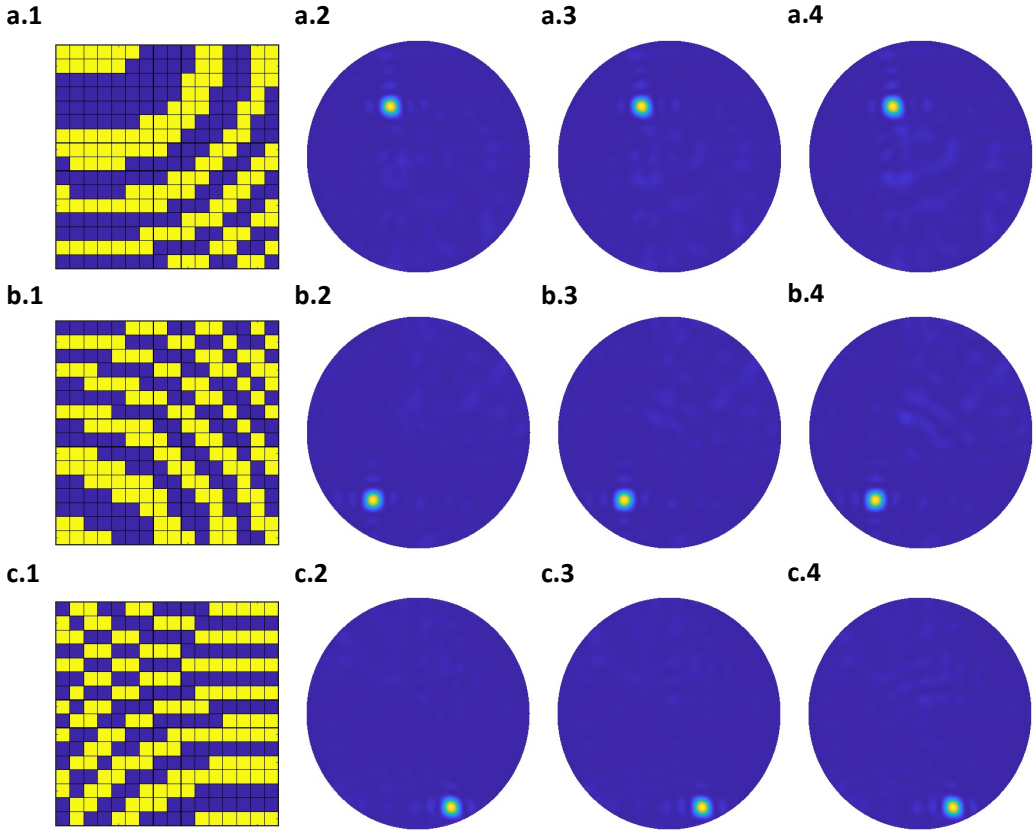

Supplementary Figure 4 The optimal codebooks and corresponding radiation patterns under different directions of main lobes (rows) and different phase biases (columns).

The codebook and its inverted codebook have the same radiation patterns under 1-bit phase factor quantization (Supplementary Figure 5). As a result, more than half of the units are always in the "ON" state.

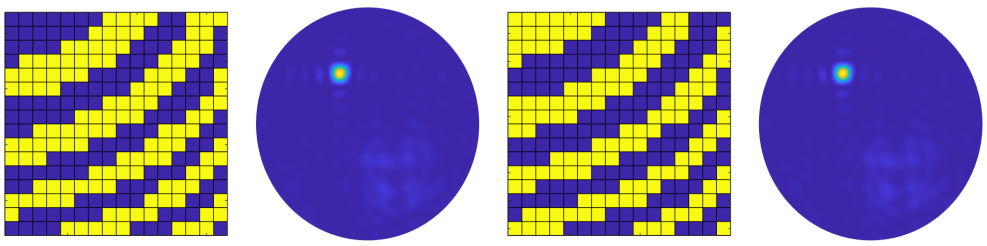

Supplementary Figure 5 The codebook and its inverted codebook have the same radiation pattern.

[1] Xiong, R., Dong, X., Mi, T., Wan, K., & Qiu, R. C. (2024, April). Optimal discrete beamforming of RIS-aided wireless communications: An inner product maximization approach. In *2024 IEEE Wireless Communications and Networking Conference (WCNC)* (pp. 1-6). IEEE.

Supplementary Note 5. Received waveforms and our designed UI of system

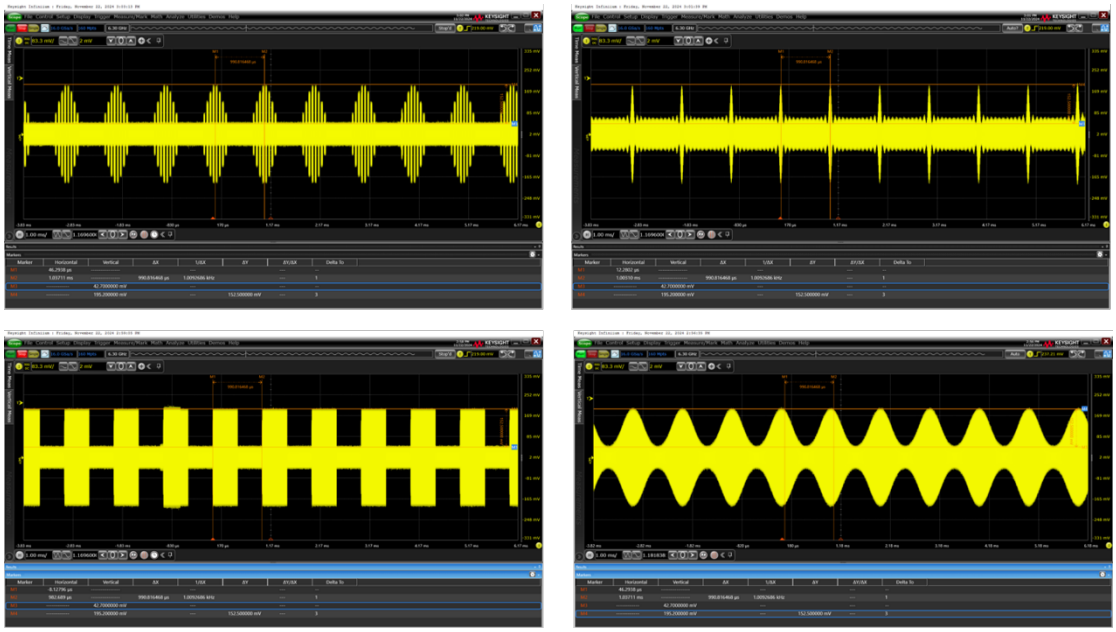

Supplementary Figure 6 Screenshots of the oscilloscope while different waveforms are modulated onto the envelope of reflected EM wave.

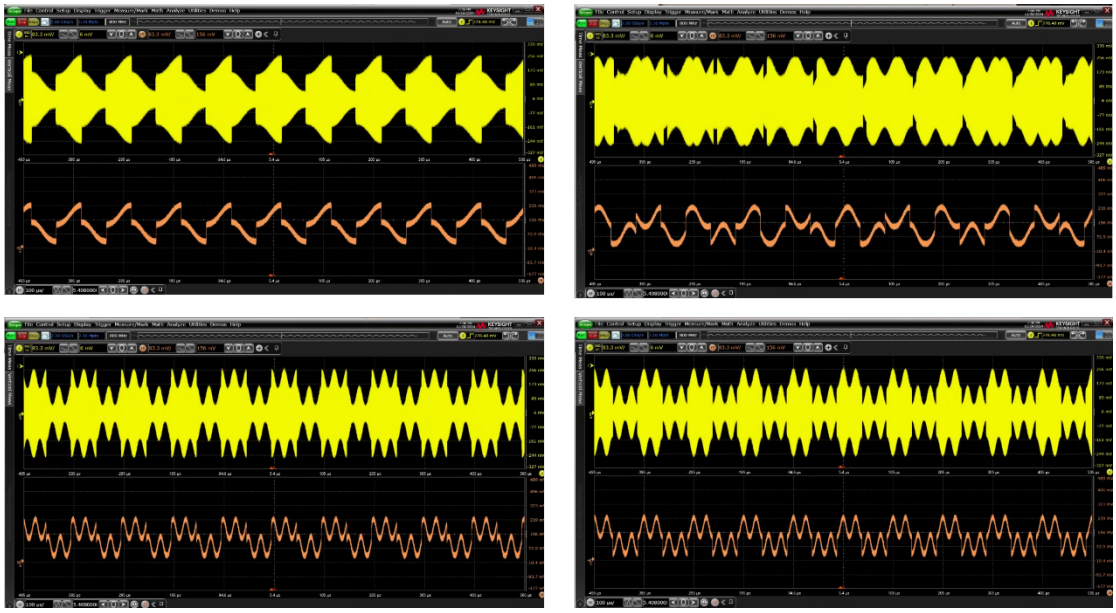

Supplementary Figure 7 Screenshots of the oscilloscope shows that the combination of two scaled or delayed waveforms generated by two inputs .

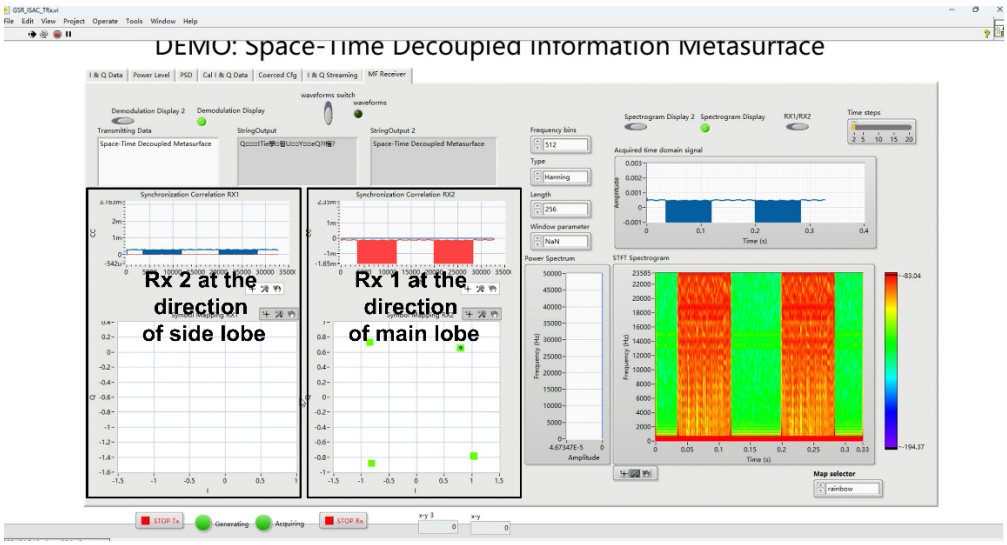

Supplementary Figure 8 Screenshot of LabView UI (Reconfigurable backscatter transmitter)

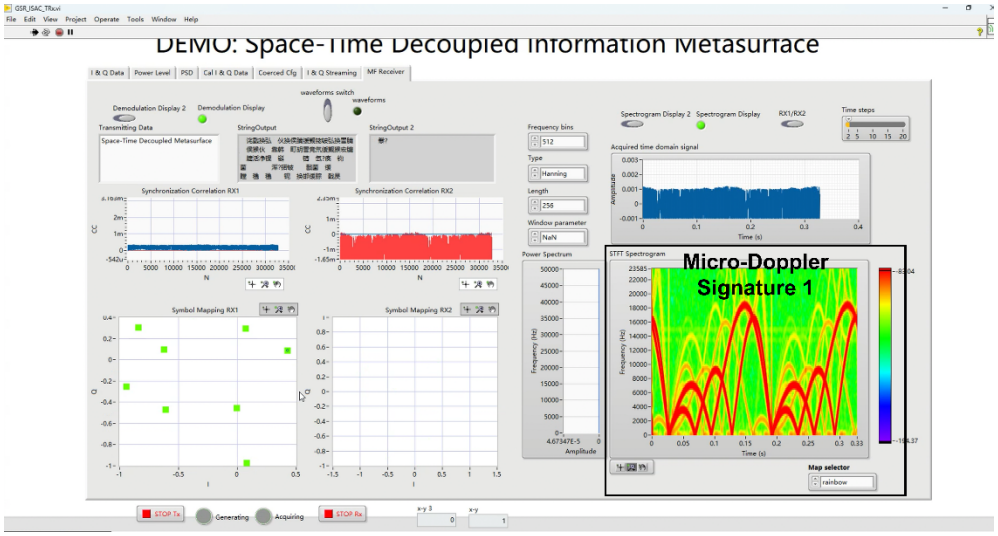

Supplementary Figure 9 Screenshot of LabView UI, micro-Doppler signature 1 (Dynamic Doppler-spoofing Reflection Array)

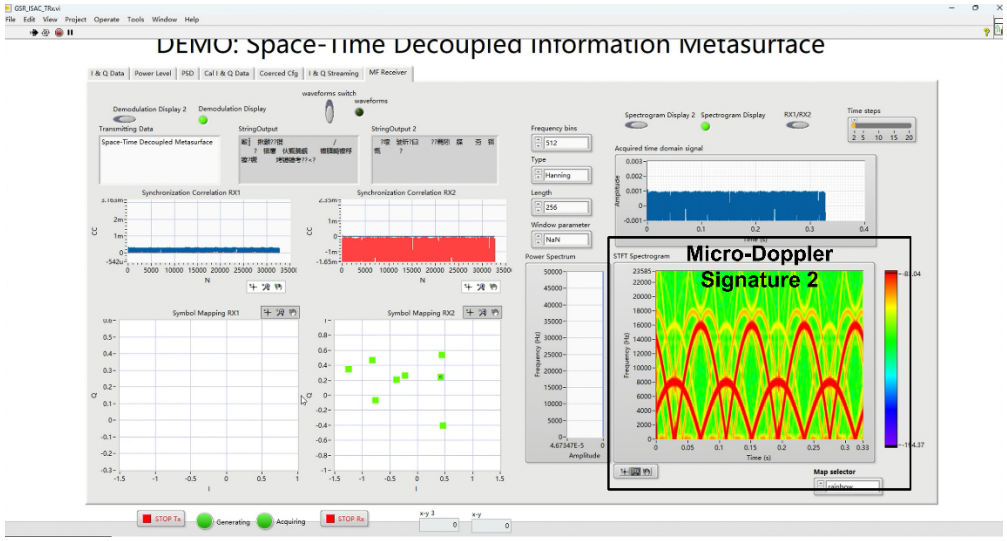

Supplementary Figure 10 Screenshot of LabView UI, micro-Doppler signature 2 (Dynamic Doppler-spoofing Reflection Array)

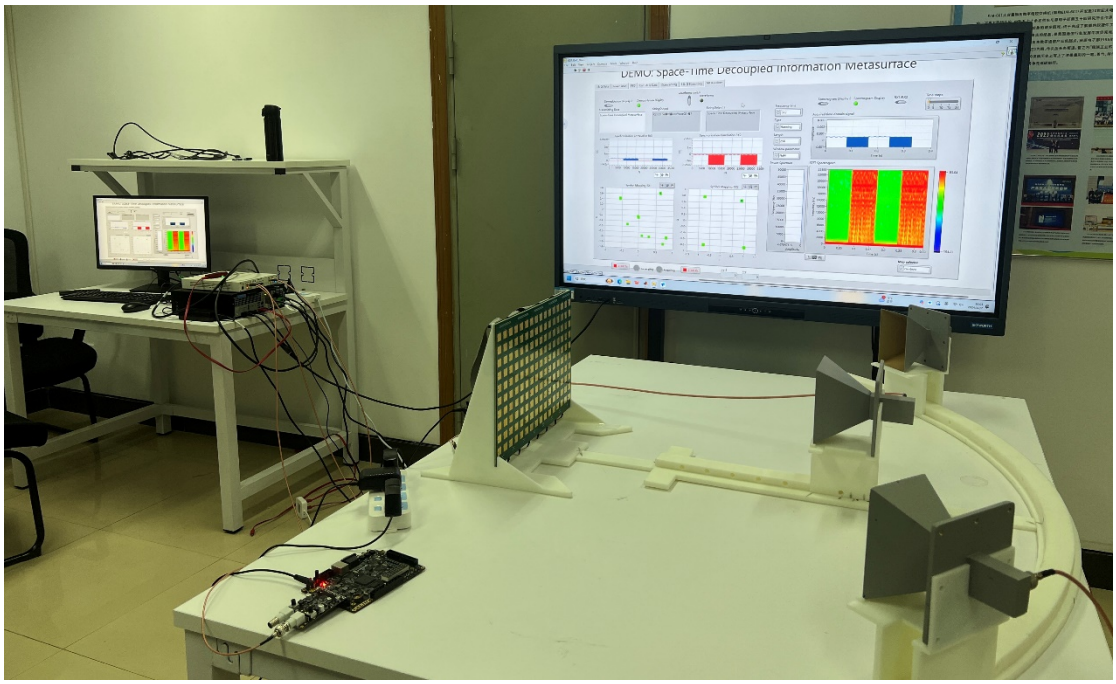

Supplementary Figure 11 The experimental setting for the applications.

Descriptions about Video Demos:

Video 1. Single input: arbitrary waveform modulation by STD-Metasurface

This demonstration is consistent with the experimental setup depicted in Figure 3(a). The horn antenna positioned directly in front of the STD metasurface transmits a monochromatic carrier at 5.7 GHz. The baseband waveforms are modulated on the envelope of the reflected electromagnetic (EM) waves. Concurrently, the main lobe of the reflected EM waves is directed towards the receiving horn antenna.

The oscilloscope displays the real-time waveform through radio frequency (RF) direct sampling, along with its envelope, which is identical to the input voltage signals.

Video 2. Over-the-air combination of two scaled waveforms

This demonstration is consistent with the experimental setup depicted in Figure 3(c). The combination of two scaled or delayed waveforms generated by two inputs, which

validates superposition principle over the air. Concurrently, the main lobe of the reflected EM waves is directed towards the receiving horn antenna.

The oscilloscope displays the real-time waveform through radio frequency (RF) direct sampling, along with its envelope, which is identical to the corresponding superpositions of two input voltage signals.

Video 3. Simultaneous beamforming and modulation

The video demonstrates that the shape of the received signals remains unaltered despite a change in the radiation pattern. This indicates that the baseband signal has been modulated onto the reflected electromagnetic (EM) waves, rendering it independent of the reflected radiation pattern. This independence is indicative of the space-time decoupling defined in the Supplementary Note 1.

Video 4. Backscatter communication and Micro-Doppler signature generation

In this video, we demonstrate the implementation of two applications: backscatter communication and micro-Doppler signature generation.

In the beamforming configuration, the main lobe of beampattern was directed towards the RX2, while the side lobe was directed towards the RX1.

In the initial stage of the experiment, no signal was introduced into the analog signal port. Subsequently, the signal output of the DAC was altered to the waveform of text. The RX2 was able to correctly decode the text "Space-Time Decoupled Metasurface," whereas the RX1 was unable to do so due to the low signal-to-noise ratio (SNR).

Subsequently, two waveforms with disparate micro-Doppler signatures, as illustrated in the right section of the LabView user interface, were alternately presented.